12th International Symposium on Turbulence and Shear Flow Phenomena (TSFP12)
Osaka, Japan (Online), July 19-22, 2022

ACTIVE TURBULENCE AND ITS MODELING

Benjamin Deußen
Chair of Fluid Dynamics
Technical Univerity of Darmstadt
Otto-Berndt-Str. 2, D-64287 Darmstadt, Germany
deussen@fdy.tu-darmstadt.de

Martin Oberlack
Chair of Fluid Dynamics
Technical Univerity of Darmstadt
Otto-Berndt-Str. 2, D-64287 Darmstadt, Germany
oberlack@fdy.tu-darmstadt.de

Yongqi Wang
Chair of Fluid Dynamics
Technical Univerity of Darmstadt
Otto-Berndt-Str. 2, D-64287 Darmstadt, Germany
wang@fdy.tu-darmstadt.de

ABSTRACT

Two dimensional active suspensions are examined. The suspension consists of a Newtonian fluid and multiple identical active Janus particles. Janus particles are a model for biological or artificial particles capable of driving themselves forward. The length of such a particle lies in the range of a few micrometers, hence, the Reynolds number $Re \ll 1$ is small. Due to the chaotic behaviour of the particles in suspensions, some authors have used the term active turbulence to describe this behaviour.

The similarities and differences between active and hydrodynamic turbulence are examined. We will use statistical moment equations and direct numerical simulations (DNS) to obtain results. The results are quantified with the help of statistical measures, such as the probability density function (PDF) and the mean values of the physical quantities.

INTRODUCTION

Active suspension consists of a fluid, which is usually but not necessarily Newtonian, and a large number N of active particles. The latter term describes objects, which are capable of driving themselves forward (Bechinger *et al.*, 2016). In general, there is no size restriction, i.e. flocks of birds or swarming fish can be described as active particles as well as bacteria or artificial microscopic objects, however, our focus lies on microscopic active particles. The simplest realisation of an artificial active particle is the Janus particle (Sharan *et al.*, 2020), which is driven forward by the chemical potential created by two different surface coatings. More complex structures are described as microrobots (Zhang *et al.*, 2019; Yigit *et al.*, 2020). Possible fields of application are environmental monitoring and cleaning (Soler & Sánchez, 2014; Jurado-Sánchez *et al.*, 2015; Orozco *et al.*, 2016) and self-healing electronics (Li *et al.*, 2015).

Colonies of motile strains of *Escherichia coli* or *Bacillus subtilis* are often used as model organisms to examine the behaviour of active particles (Wu & Libchaber, 2000; Drescher *et al.*, 2011; Sokolov & Aranson, 2012; Dombrowski *et al.*, 2004). Important parameters for the characteristics of the collective behaviour of an active suspension are the density of the suspension (Baskaran & Marchetti, 2009), the shape of the particles (Wensink *et al.*, 2012; Be'er *et al.*, 2020) and the enclosure of the entire system (Wu *et al.*, 2017; Dhar *et al.*, 2020). For high particle densities the flow pattern shows similarities to hydrodynamic turbulence, which leads to the occasionally used term "active turbulence" (Bratanov *et al.*, 2015; Alert *et al.*, 2022). While both phenomena - active and hydrodynamic turbulence - show similarities, the differences are evident. Hydrodynamic turbulence only occurs in systems with a very large Reynolds number, whereas active suspensions with microscopic particles exist in a regime of very low Reynolds numbers $Re \ll 1$. Hence, hydrodynamic turbulent flows are governed by inertia and active suspensions by viscosity.

GOVERNING EQUATIONS

A general, incompressible, Newtonian fluid is described by the Navier-Stokes equation

$$\frac{\partial u_i^F}{\partial t} + \frac{\partial u_i^F u_j^F}{\partial x_j} = -\frac{\partial p^F}{\partial x_i} + \frac{1}{Re}\frac{\partial^2 u_i^F}{\partial x_j^2}, \tag{1}$$

where u_i^F is the fluid velocity and p^F the fluid pressure. Due to the low Reynolds number the convective term $\partial u_i^F u_j^F / \partial x_j$ is small compared to the viscous term, hence, it can be neglected, leading to the unsteady Stokes equation

$$\frac{\partial u_i^F}{\partial t} = -\frac{\partial p^F}{\partial x_i} + \frac{1}{Re}\frac{\partial^2 u_i^F}{\partial x_j^2}. \tag{2}$$

Applying the rotation operator to (2) delivers the equation for the vorticity ω^F

$$\frac{\partial \omega_i^F}{\partial t} = \frac{1}{Re}\frac{\partial^2 \omega_i^F}{\partial x_j^2}. \tag{3}$$

The vortex stretching term $\omega_j^F \left(\partial u_i^F / \partial x_j\right)$ does not occur in (3) as it is a result of the convective term in (1). Subsequently,

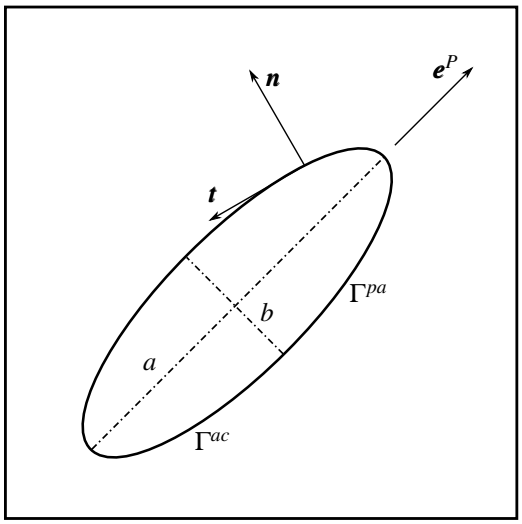

Figure 1. A two dimensional Janus particle. The surface of the particle is split by the shorter axis b into a passive Γ^{pa} and an active part Γ^{pa}.

the energy cascade of three dimensional hydrodynamic turbulence will not occur in an low-Reynolds active suspension regardless of the spatial dimension. Furthermore, as the injection of energy into the system is on the same scale as the dissipation, which dominates all scales of an active suspension, no energy cascade is expected to occur (Alert *et al.*, 2022).

The motion of the particles is described by the Newton-Euler equations for rigid particles, where we will restrict ourselves to two dimensions

$$m^P \frac{\mathrm{d}v_i^P}{\mathrm{d}t} = \int_{\Gamma^P} \tau_{ij}^F n_j \,\mathrm{d}s, \tag{4}$$

$$\Theta^P \frac{\mathrm{d}\omega^P}{\mathrm{d}t} = \int_{\Gamma^P} \varepsilon_{3ij} \left(x_i - \chi_i^P\right) \tau_{jk}^F n_k \,\mathrm{d}s. \tag{5}$$

Here, v_i^P is the translational velocity of the particle P, ω^P is the rotational velocity, χ_i^P is the position of the centre of mass, m^P is the mass and Θ^P the moment of inertia and n_i is the outward pointing normal vector at the particle surface Γ^P. The fluid stress tensor

$$\tau_{ij}^F = -p^F \delta_{ij} + \frac{1}{Re}\left(\frac{\partial u_i^F}{\partial x_j} + \frac{\partial u_j^F}{\partial x_i}\right) \tag{6}$$

is the source of momentum for the the particles.

The equations (4) and (5) are valid for active and passive particles. The capability of self-driven motion is introduced into our model by the means of an active boundary condition. The particle surface is split into two parts by the shorter half axis b (Fig. 1), i.e. our model is a so called Janus particle. At the passive part Γ^{pa} of the boundary a no-slip condition is applied. Hence, the local particle and fluid velocity are equal

$$u_i^F = u_i^P = v_i^P + \varepsilon_{i3j}\omega^P \left(x_j - \chi_j^P\right) \quad \forall \boldsymbol{x} \in \Gamma^{pa}. \tag{7}$$

The surface of the particle is impermeable, thus, at the active part of the surface Γ^{ac} the condition

$$u_i^F n_i = u_i^P n_i \quad \forall \boldsymbol{x} \in \Gamma^{ac}. \tag{8}$$

must be fulfilled. Furthermore, a mechanical stress is applied, which permits a slip velocity in the tangential direction. The tangential vector t_i is defined as

$$t_i = \varepsilon_{ijk}\left(\varepsilon_{jlm} e_l^P n_m\right) n_k, \tag{9}$$

where e_i^P is the orientation vector of the particle, see Fig. 1. Due to its definition the tangential vector points always in the backwards direction $e_i^P t_i \leq 0$ of the particle. Hence, the active stress is

$$f_i^{ac} = A_c t_i \quad \forall \boldsymbol{x} \in \Gamma^{ac}, \tag{10}$$

where A_c is the constant non-dimensional active stress magnitude. Subsequently, the fluid at the active boundary is accelerated in the backwards direction. Due to momentum conservation the resulting reaction force of the fluid will accelerate the particle in the direction of e_i^P by the means of the integral term in (4).

Eulerian spatial averaging theory

To get a first impression of the behaviour of an active suspension we use volume-averaged equations. The underlying idea of Eulerian spatial averaging theory, see e.g. Drew (1983), is to express all physical variables in terms of their averages

$$\left\langle \psi^{\mathfrak{P}} \right\rangle (\boldsymbol{x},t) = \frac{1}{V}\int_V \psi^{\mathfrak{P}}(\boldsymbol{r},t)\,\gamma^{\mathfrak{P}}(\boldsymbol{r},t)\,\mathrm{d}V, \tag{11}$$

where $\mathfrak{P}$ indicates an arbitrary phase, $\psi^{\mathfrak{P}}$ an arbitrary physical variable of the given phase and V the respective averaging volume. Note that V needs to be sufficiently larger than the particle volume but also much smaller than the entire computational domain. The function $\gamma^{\mathfrak{P}}$ is the phase indicator function which is defined as

$$\gamma^{\mathfrak{P}}(\boldsymbol{x},t) = \begin{cases} 1 & \boldsymbol{x} \in V^{\mathfrak{P}} \\ 0 & \boldsymbol{x} \notin V^{\mathfrak{P}}, \end{cases} \tag{12}$$

where $V^{\mathfrak{P}}$ is the volume occupied by the phase $\mathfrak{P}$.

Due to the average each phase is present at each space-time point $(\boldsymbol{x},t)$, hence it is necessary to solve the equations for both phases simultaneously. Furthermore, we have the saturation condition

$$\alpha^S + \alpha^F = 1, \tag{13}$$

where $\alpha^S = \frac{V^S}{V}$ is the volume fraction of the particle phase and $\alpha^F = \frac{V^F}{V}$ is the volume fraction of the fluid phase. Using the respective volume fractions, we introduce the average over the volume occupied by a single phase $\overline{\psi^{\mathfrak{P}}} = \left\langle \psi^{\mathfrak{P}} \right\rangle / \alpha^{\mathfrak{P}}$, which we call true physical average.

Using the volume average (11) to derive balance equations for the mass, linear and angular momentum for both

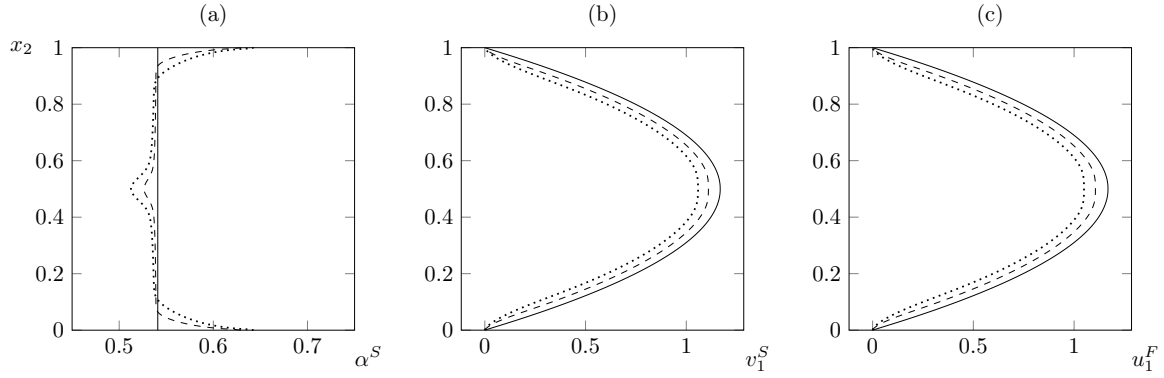

Figure 2. Results obtained for a pressure and active stress driven channel flow. (a) Profiles of the the solid phase volume fraction α^S. (b) Averaged particle translational x_1-velocity v_1^S. (c) Averaged fluid x_1-velocity u_1^F. On the vertical axis the remaining spatial coordinate vertical to the channel is denoted. Results are plotted for $\mathfrak{A}_c = 0$ (——), $\mathfrak{A}_c = 500$ (- - -) and $\mathfrak{A}_c = 1000$ (⋯). Figure reproduce from Deußen *et al.* (2022), Fig. 8a-c.

phases and an equation for the averaged orientation of the particle phase delivers in two dimensions

$$\frac{\partial \alpha^S}{\partial t} + \frac{\partial \alpha^S \overline{v_i^S}}{\partial x_i} = 0, \quad \frac{\partial \alpha^F}{\partial t} + \frac{\partial \alpha^F \overline{u_i^F}}{\partial x_i} = 0 \tag{14}$$

$$\frac{\partial \alpha^F \overline{u_i^F}}{\partial t} + \frac{\partial \alpha^F \overline{u_i^F}\,\overline{u_j^F}}{\partial x_j} = -\frac{\partial \alpha^F \overline{p^F}}{\partial x_i} + \frac{1}{Re^F}\frac{\partial}{\partial x_j}\alpha^S\left[\frac{\partial \overline{u_i^F}}{\partial x_j} + \frac{\partial \overline{u_j^F}}{\partial x_i}\right] + \langle F_i \rangle = 0, \tag{15}$$

$$\mathfrak{D}\left[\frac{\partial \alpha^S \overline{v_i^S}}{\partial t} + \frac{\partial \alpha^S \overline{v_i^S}\,\overline{v_j^S}}{\partial x_j} + \frac{2}{3}\frac{\partial \alpha^S \overline{K}}{\partial x_i} - \frac{\partial}{\partial x_j}\left[\alpha^S \mu^S \left(\frac{\partial \overline{v_i^S}}{\partial x_j} + \frac{\partial \overline{v_j^S}}{\partial x_i}\right)\right]\right] - \langle F_i \rangle = 0, \tag{16}$$

$$\Theta^S\left[\frac{\partial \alpha^S \overline{\omega^S}}{\partial t} + \frac{\partial \alpha^S \overline{\omega^S}\,\overline{v_i^S}}{\partial x_i} + \frac{2}{3}\frac{\partial \alpha^S \overline{W}_i}{\partial x_i} - \frac{\partial}{\partial x_i}\left(\alpha^S \mu^S \frac{\partial \overline{\omega^S}}{\partial x_i}\right)\right] - \langle T \rangle = 0, \tag{17}$$

$$\frac{\partial \alpha^S \overline{e_i^S}}{\partial t} + \frac{\partial \alpha^S \overline{e_i^S}\,\overline{v_j^S}}{\partial x_j} - \frac{\partial}{\partial x_i}\frac{\alpha^S \mathfrak{A}_c a Re^M}{96\pi\lambda^2} - \frac{\partial}{\partial x_j}\left[\alpha^S \mu^S \left(\frac{\partial \overline{e_i^S}}{\partial x_j} + \frac{\partial \overline{e_j^S}}{\partial x_i}\right)\right] - \alpha^S \varepsilon_{i3k}\overline{\omega^S}\,\overline{e_k^S} = 0. \tag{18}$$

Here, $\overline{u_i^F}$ and $\overline{p^F}$ are the mean fluid velocity and pressure, $\overline{v_i^S}$, $\overline{\omega^S}$ and $\overline{e_i^S}$ are the mean translational and rotational particle velocity and the particle orientation. Additional terms arise due to the interactions between the phases; $\langle F_i \rangle$ represents interaction forces and $\langle T \rangle$ interaction torques. The two quantities $\overline{K}$ and $\overline{W}$ represent interactions between the particles and between particles and the wall based on the averaged active force $\mathfrak{A}_c = \frac{2aA_c}{\varepsilon V^F}\int_{\frac{\pi}{2}}^{\pi} \sin(\sigma)\sqrt{\varepsilon^2 \sin^2(\sigma) + \cos^2(\sigma)}d\sigma$. An in depth derivation of the given equation can be found in Deußen *et al.* (2022).

Results

The model is used to obtain results for a planar Poiseuille channel flow. To obtain results MATLAB (Version 9.2.0.556344, R2017a) is used. The equations are solved using the partial differential equations solver *pdepe.m*, employing finite differences (Skeel & Berzins, 1990) for the spatial discretisation and numerical differentiation formulas for the time discretisation, implemented by *ode15s.m* (Shampine & Reichelt, 1997; Shampine *et al.*, 1999). The respective MATLAB-scripts are publicly available at TUdatalib (Deußen *et al.*, 2021). The results were, together with further setups, first presented in Deußen *et al.* (2022).

The results presented in Fig. 2 show a quasi steady state, where the averaged vertical velocities are negligibly small compared to the velocities parallel to the channel wall and are not displayed here. The flow is driven by a pressure gradient $\partial \overline{p^F}/\partial x_1 = -10^6$ and the active force of the particles. Three numerical experiments are carried out with varying averaged active forces $\mathfrak{A}_c = 0$, $\mathfrak{A}_c = 500$ and $\mathfrak{A}_c = 1000$.

In case of the passive suspension $\mathfrak{A}_c = 0$ the parabolic velocity profile of an Newtonian fluid is retrieved. Due to the low Reynolds number the particles follow the stream lines of the fluid. Negligible forces in the vertical direction are observed, hence, the volume fraction α^S does not change in space, see Fig. 2a.

Despite the expected chaotic behaviour clear structures emerge in results for the averaged quantities of the active suspensions. As visible in Fig. 2a material accumulates at the channel walls for active suspensions. The reason for this accumulation are twofold. For once, active particles have an inherent tendency to accumulate at solid walls (Bechinger *et al.*, 2016; Berke *et al.*, 2008). This is represented by the term $\overline{K}$ in the equation for the averaged linear momentum (16) of the particles, see Deußen *et al.* (2022) for a more detailed discussion and derivation. The second reason for the accumulation is the averaged Saffman-force, acting on the particles perpendicular to the relative velocity $\overline{w_i^S} = \left(\overline{u_i^F} - \overline{v_i^S}\right)$ and rotation $\overline{\omega_i} = \left(0.5\overline{\omega_i^F} - \overline{\omega_i^S}\right)$ between the two phases (Deußen *et al.*, 2022)

$$\left\langle F_i^{LS} \right\rangle = 1.615\alpha^S \sqrt{\frac{a}{Re^M}}\,|\overline{\boldsymbol{\omega}}|^{-\frac{1}{2}}\,\varepsilon_{ijk}\overline{w_j^S}\,\overline{\omega_k}, \tag{19}$$

The averaged relative velocity $\overline{w_i^S}$ is caused by the active force,

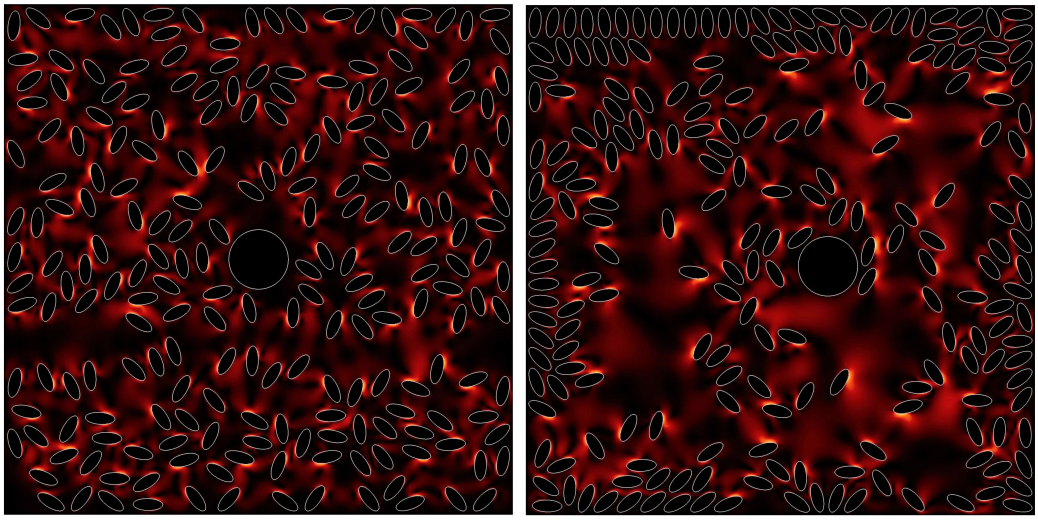

Figure 3. Snapshots of a DNS with 211 active particles and a single passive particle. The left figure shows the situation at $t = 20$, the right figure shows the same domain at $t = 100$. The particles form clusters cluster alongside the wall and to a lesser extent in the proximity of the passive disk-shaped particle.

thus, this effect is not visible in a passive suspension. In fact there are several studies (Leighton & Acrivos, 1985; Derksen & Larsen, 2011; Agudo *et al.*, 2017), which show that the Saffman force is negligible for the case of passive spheres.

The profiles for the velocity of the two phases in case of the active suspension show an area of reduced velocity gradients at the channel walls. This is caused by the accumulation of material. In the limiting case, where α^S reaches the maximal packing fraction, the suspension will behave like a solid, leading to a vanishing velocity gradient. The overall velocity of the active suspension is reduced, compared to the passive suspension. The main reason is the additional stress between the two phases. This effect may be somewhat resembling the behaviour of a turbulent flow, where increased stresses provide a flatter velocity profile. Obviously, however, the cause for the similar behaviour is different. In the case of hydrodynamic turbulence, one has to deal with increased internal stresses, which become visible as Reynolds stresses in the averaged Navier-Stokes equations. In contrast, the active stresses are a material parameter of the active suspension.

DIRECT NUMERICAL SIMULATIONS

The model system consisting of the unsteady Stokes equation (2) and the Newton-Euler equations (4) and (5) is implemented into the *Bo*unded *S*upport *S*pectral *S*olver (BoSSS) framework [1] (Kummer *et al.*, 2021). This framework provides high-order discontinuous Galerkin (DG) methods to solve the fluid phase of the suspension. Within this framework it is possible to represent the particle surface with sub-cell accuracy by employing a level-set method, implemented by the extend discontinuous Galerkin method (XDG) (Kummer, 2017; Kummer *et al.*, 2018).

We present results for a closed system of 211 active particles and a single passive particle. The length of the active particles is $a^{ac} = 1$, the aspect ratio is $\varepsilon = 5/2$ and the active stress magnitude $A_c = 10$. The passive particle is a disk with a diameter $a^{pa} = 2$. The simulation is carried out in a 18×18 domain with the mesh size $h = 1/12$. Fig. 3 shows the simulation progress between $t = 20$ and $t = 100$. From an approximatly

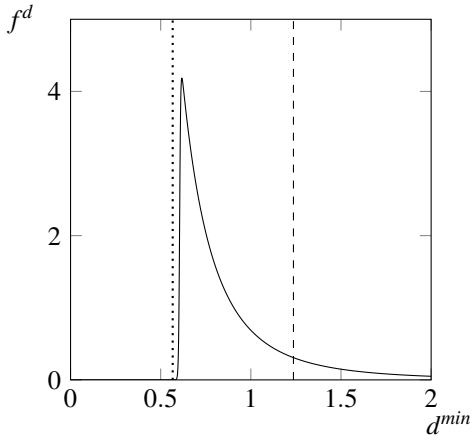

Figure 4. The PDF f^d for the minimal distance between two particles is marked by (——). The lower limit for the PDF is the particle dimension plus the minimal distance threshold, marked by (· · · ·). In case that all particles would be equally distributed in the domain, the distance between each particle would be $d = 1.24$ (- - -).

uniform distribution at the first time the particle form clusters at the second time. These clusters mainly form at the domain walls and are, thus, similar to the results of the volume averaged simulation. However, they also appear within the domain and in proximity to the passive particle.

We analyse the behaviour of the particles using probability density functions (PDF), obtained by using the MATLAB function *fitdist*. As a measure of the clustering phenomenon, a PDF for the minimal distance f^d between two particle centres of mass is introduced, see Fig. 4. This PDF returns the probability of finding a second particle at a certain distance from a probing particle. It clearly shows that the highest probability is in the closest proximity of the probing particle. Hence, the visual impression of cluster formation obtained from the snapshots in Fig. 3 can be confirmed by the PDF. In case of a hypothetical uniform distribution, the distance between the particles would overall be larger, as indicated by the dashed line in Fig. 4. Hence, clear structures are formed in contrast to

[1] Openly available at https://github.com/FDYdarmstadt/BoSSS

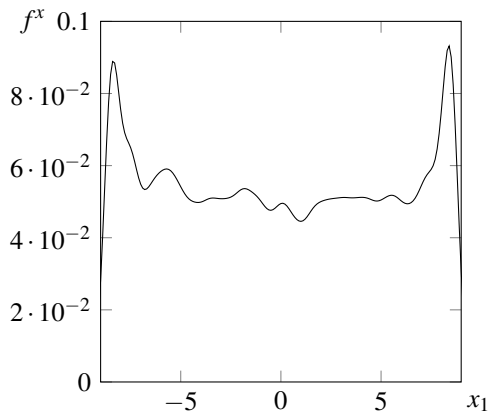

Figure 5. The PDF f^x for the x_1-coordinate of the position of the particles within the domain. The results are preliminary. With a longer run-time of the simulation and thus additional data, it is to be expected that f^x is constant within the domain and only two peaks form on the walls, which are already recognisable in the available smaller data set.

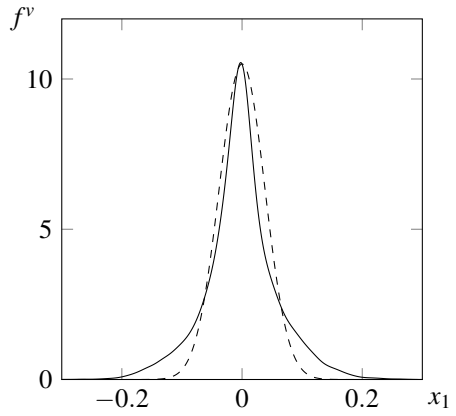

Figure 6. The PDF f^v for the particle translation x_1-velocity (——). While the PDF might look Gaussian, the comparison with a normal distribution (- - -) reveals that especially for larger possible velocities it is non-Gaussian.

the idea of a chaotic behaviour.

The increase of α^S in the volume averaged simulation at the channel walls can also be observed in the DNS-simulation. The PDF f^x (Fig. 5) gives the probability of finding a particle centre of mass at a certain x_1-coordinate of the domain. It should be noted, that the data shown in Fig. 5 are preliminary, a steady state has not jet been reached. Nevertheless, it already indicate what is to expected from the final data. Within the domain the distribution will be constant, whereas material accumulated at the domain wall, leading to the two peaks visible in f^x.

While the PDFs for the minimal distance f^d and position f^x indicate a structured behaviour, i.e. the formation of clusters, the analysis of the velocity PDF reveals a more chaotic behaviour. In Fig. 6 the PDF for the v_1-velocity of the particles is plotted. Non-Gaussian "heavy tails" are clearly visible, resembling the behaviour of a turbulent flow, see for example Wilczek & Friedrich (2009). This non-Gaussian behaviour could indicate that effects such as intermittency are occurring; a phenomenon that is often studied in turbulence research based on vorticity (Li & Meneveau, 2005).

DISCUSSION

Structures are made visible with both models. Active particles have a tendency to attach to walls, as is visible in the case of both, the volume-averaged model and the DNS. This attraction is due solely to the active stress at the surface, as it does not occur in the case of passive suspension. Furthermore, loose clusters are also formed in the domain, as can be seen from the snapshots of the DNS. In this sense, active suspensions thus behave in a predictable and less chaotic manner.

The observation of the velocity PDF shows a non-Gaussian behaviour. This shows similarities with the non-Gaussianity in the case of hydrodynamic turbulence and possibly indicates the phenomenon of intermittency. Further analysis in this regard is needed. Intermittency, i.e. the sudden occurrence of a chaotic state in an otherwise ordered system, thus indicates a behaviour similar to hydrodynamic turbulence. It should be noted, however, that in an active system there is no classical energy cascade, as can be easily shown by considering the vorticity equation. Considering the energy cascade as defining property of hydrodynamic turbulence, the term active turbulence might be misleading from the standpoint of fluid mechanics. Nevertheless, applying techniques known from hydrodynamic turbulence research to active suspension might lead to interesting new results as shown for example by Deußen *et al.* (2021).

REFERENCES

Agudo, JR, Illigmann, C, Luzi, G, Laukart, A, Delgado, A & Wierschem, A 2017 Shear-induced incipient motion of a single sphere on uniform substrates at low particle reynolds numbers. *J. Fluid Mech.* **825**, 284–314.

Alert, R., Casademunt, J. & Joanny, J-F 2022 Active turbulence. *Annual Review of Condensed Matter Physics* **13**, 143–170.

Baskaran, A. & Marchetti, M. C. 2009 Statistical mechanics and hydrodynamics of bacterial suspensions. *Proc. Natl. Acad. Sci. USA* **106** (37), 15567–15572.

Bechinger, C., Di Leonardo, R., Löwen, H., Reichhardt, C., Volpe, G. & Volpe, G. 2016 Active particles in complex and crowded environments. *Rev. Mod. Phys.* **88**, 045006.

Be'er, A., Ilkanaiv, B., Gross, R., Kearns, D. B., Heidenreich, S., Bär, M. & Ariel, G. 2020 A phase diagram for bacterial swarming. *Commun. Phys.* **3** (1), 66.

Berke, A. P., Turner, L., Berg, H. C. & Lauga, E. 2008 Hydrodynamic attraction of swimming microorganisms by surfaces. *Phys. Rev. Lett.* **101** (3), 038102.

Bratanov, V., Jenko, F. & Frey, E. 2015 New class of turbulence in active fluids. *Proc. Natl. Acad. Sci. USA* **112** (49), 15048–15053.

Derksen, JJ & Larsen, RA 2011 Drag and lift forces on random assemblies of wall-attached spheres in low-reynolds-number shear flow. *J. Fluid Mech.* **673**, 548–573.

Deußen, B., Oberlack, M. & Wang, Y. 2021 Probability theory of active suspensions. *Phys. Fluids* **33** (6), 061902.

Deußen, Benjamin, Wang, Yongqi & Oberlack, Martin 2022 A deterministic two-phase model for an active suspension with non-spherical active particles using the eulerian spatial averaging theory. *Physics of Fluids* **34** (2), 023302.

Deußen, B., Wang, Y. & Oberlack, M. 2021 A deterministic two-phase model for an active suspension with non-spherical active particles using eulerian spatial averaging theory. TUdatalib, Dataset, https://doi.org/10.48328/tudatalib-781.

Dhar, A., Burada, P. S. & Sekhar, G. P. Raja 2020 Hydrody-

namics of active particles confined in a periodically tapered channel. *Phys. Fluids* **32** (10), 102005.

Dombrowski, C., Cisneros, L., Chatkaew, S., Goldstein, R. E. & Kessler, J. O. 2004 Self-concentration and large-scale coherence in bacterial dynamics. *Phys. Rev. Lett.* **93**, 098103.

Drescher, K., Dunkel, J., Cisneros, L. H., Ganguly, S. & Goldstein, R. E. 2011 Fluid dynamics and noise in bacterial cell–cell and cell–surface scattering. *Proc. Natl. Acad. Sci. USA* **108** (27), 10940–10945.

Drew, D. A. 1983 Mathematical modeling of two-phase flow. *Annu. Rev. Fluid Mech.* **15** (1), 261–291.

Jurado-Sánchez, B., Sattayasamitsathit, S., Gao, W., Santos, L., Fedorak, Y., Singh, V. V., Orozco, J., Galarnyk, M. & Wang, J. 2015 Self-propelled activated carbon janus micromotors for efficient water purification. *Small* **11** (4), 499–506.

Kummer, F. 2017 Extended discontinuous galerkin methods for two-phase flows: the spatial discretization. *International Journal for Numerical Methods in Engineering* **109** (2), 259–289.

Kummer, F., Müller, B. & Utz, T. 2018 Time integration for extended discontinuous galerkin methods with moving domains. *Int. J. Numer. Methods Eng.* **113** (5), 767–788.

Kummer, F., Weber, J. & Smuda, M. 2021 Bosss: A package for multigrid extended discontinuous galerkin methods. *Comput. Math. with Appl.* **81**, 237–257.

Leighton, David & Acrivos, Andreas 1985 The lift on a small sphere touching a plane in the presence of a simple shear flow. *Z. Angew. Math. Phys.* **36** (1), 174–178.

Li, Jinxing, Shklyaev, Oleg E, Li, Tianlong, Liu, Wenjuan, Shum, Henry, Rozen, Isaac, Balazs, Anna C & Wang, Joseph 2015 Self-propelled nanomotors autonomously seek and repair cracks. *Nano Letters* **15** (10), 7077–7085.

Li, Yi & Meneveau, Charles 2005 Origin of non-gaussian statistics in hydrodynamic turbulence. *Physical review letters* **95** (16), 164502.

Orozco, Jahir, Mercante, Luiza A, Pol, Roberto & Merkoçi, Arben 2016 Graphene-based janus micromotors for the dynamic removal of pollutants. *J. Mater. Chem. A* **4** (9), 3371–3378.

Shampine, Lawrence F & Reichelt, Mark W 1997 The matlab ode suite. *SIAM J. Sci. Comput.* **18** (1), 1–22.

Shampine, Lawrence F, Reichelt, Mark W & Kierzenka, Jacek A 1999 Solving index-1 daes in matlab and simulink. *SIAM Rev.* **41** (3), 538–552.

Sharan, Priyanka, Postek, Witold, Gemming, Thomas, Garstecki, Piotr & Simmchen, Juliane 2020 Study of active janus particles in the presence of an engineered oil–water interface. *Langmuir* .

Skeel, Robert D & Berzins, Martin 1990 A method for the spatial discretization of parabolic equations in one space variable. *SIAM J. Sci. Comput.* **11** (1), 1–32.

Sokolov, Andrey & Aranson, Igor S. 2012 Physical properties of collective motion in suspensions of bacteria. *Phys. Rev. Lett.* **109**, 248109.

Soler, Lluís & Sánchez, Samuel 2014 Catalytic nanomotors for environmental monitoring and water remediation. *Nanoscale* **6** (13), 7175–7182.

Wensink, Henricus H., Dunkel, Jörn, Heidenreich, Sebastian, Drescher, Knut, Goldstein, Raymond E., Löwen, Hartmut & Yeomans, Julia M. 2012 Meso-scale turbulence in living fluids. *Proc. Natl. Acad. Sci. USA* **109** (36), 14308–14313.

Wilczek, Michael & Friedrich, Rudolf 2009 Dynamical origins for non-gaussian vorticity distributions in turbulent flows. *Physical Review E* **80** (1), 016316.

Wu, K.-T., Hishamunda, J.B., Chen, D.T.N., DeCamp, S.J., Chang, Y.-W., Fernandez-Nieves, A., Fraden, S. & Dogic, Z. 2017 Transition from turbulent to coherent flows in confined three-dimensional active fluids. *Science* **355**.

Wu, Xiao-Lun & Libchaber, Albert 2000 Particle diffusion in a quasi-two-dimensional bacterial bath. *Phys. Rev. Lett.* **84** (13), 3017.

Yigit, Berk, Alapan, Yunus & Sitti, Metin 2020 Cohesive self-organization of mobile microrobotic swarms. *Soft Matter* **16** (8), 1996–2004.

Zhang, Zhuoran, Wang, Xian, Liu, Jun, Dai, Changsheng & Sun, Yu 2019 Robotic micromanipulation: Fundamentals and applications. *Annu. rev. control robot. auton. syst.* **2**, 181–203.